

An improved method for constructing models of self-gravitating tori around black holes

Nikolaos Stergioulas

*Department of Physics, Aristotle University of Thessaloniki
Thessaloniki 54124, Greece*

Received Day Month Year

Revised Day Month Year

Communicated by Managing Editor

General-relativistic models of self-gravitating tori around black holes are constructed with a self-consistent-field method in compactified coordinates. The numerical code is highly accurate and robust, allowing for the construction of models that exactly fill their Roche lobe, when a cusp exists. As a first application, we focus on self-consistent models with cusp, having different values of constant specific angular momentum. Scaling all results with the mass of the black hole, we find evidence that models with constant specific angular momentum that can fill their Roche lobe are still limited by $l < 4M_{\text{BH}}$ (as is the case for models constructed in a fixed background metric) even for heavy tori.

1. Introduction

Massive relativistic accretion tori around black holes (BHs) can form as transient structures in several astrophysical scenarios, including the core-collapse of massive stars^{1,2} and the merger of neutron star (NS) and NS-BH binaries^{3,4,5}. Recent numerical simulations have demonstrated that the mass of the torus resulting from binary NS-NS or BH-NS mergers, which are candidates for the central engine of short gamma-ray bursts (GRBs), can be in the range of $\sim 0.01-0.2M_{\odot}$ ^{6,7,4,5}. In addition, studies of the stability of accretion tori have revealed that they can be subject to several types of non-axisymmetric instabilities in a number of circumstances^{8,9,10,11}, which can lead to highly variable and unstable accretion rates. Nonaxisymmetric instabilities have been recently shown to also exist in fully general-relativistic models of massive accretion tori¹².

Another important instability, the axisymmetric runaway instability¹³ in models that fill their Roche lobe, has been investigated extensively. Numerical simulations in a time-varying Schwarzschild background showed that the instability is active for tori with constant specific angular momentum¹⁴. For the same class of tori, the adoption of a time-varying Kerr background resulted in longer timescales for the instability to grow, as the rotation of the black hole increased¹⁵. Adopting a power-law distribution of the specific angular momentum with (even small) positive slope stabilizes the torus against the runaway instability^{16,18,15,19}. The instability was shown to be active for constant specific angular momentum tori, even when tak-

ing self-gravity into account^{20,21}. For self-gravitating, non-constant specific angular momentum tori, the presence of the instability still depends on the slope of the specific angular momentum law, with the range shrinking as the black hole rotation increases¹⁷. When self-gravity is taken into account and the torus loses more than a few percent of its mass due to mass transfer, it was found that the instability is active for different specific angular momentum laws^{22,23}. However, more recent, fully general-relativistic simulations of some models of self-gravitating tori with either constant or non-constant specific angular momentum did not show signs of the instability on a dynamical timescale²⁴. The parameter space to be investigated for the conditions of the onset of the runaway instability is still large and there is a need for highly accurate self-consistent models, suitable as numerical initial data for simulation codes.

Analytic models of tori in a fixed spacetime were presented in Refs. 25, 26. These can serve as an initial guess for a self-consistent-field approach. Indeed, some first self-consistent models in quasi-isotropic coordinates were presented in Ref. 27, but with a numerical grid truncated at a finite outer radius. A different numerical method was used for constructing self-consistent models of uniformly rotating rings around black holes²⁸. More recently, a new numerical method was presented for constructing initial data of self-consistent models that are suitable for simulations using the moving puncture method²⁹. Since Roche-lobe filling models can have very large outer radii, compared to the radius of the central black hole and, in addition, accurate gravitational wave extraction in numerical simulations requires the outer numerical boundaries to be placed at even larger distances from the source, the task of computing accurate initial data on such different length scales is challenging, but can be met with a compactified grid. In particular, a global compactified grid can be constructed with a re-definition of the radial coordinate, as was done in Ref. 30 for models of rotating neutron stars. This type of compactification is adopted here in order to remove the limitations of the method presented in Ref. 27.

The effect of self-gravity on the properties of a black-hole torus spacetime (and on the properties of the torus itself) will, of course, directly depend on the ratio of torus mass to black hole mass. Here, we present evidence that even for heavy tori, models with constant specific angular momentum, l , can fill their Roche lobe only if it is limited by the same relation that holds for models constructed in a fixed background metric, $l < 4M_{\text{BH}}$, where M_{BH} is the mass of the black hole.

The paper is organized as follows: In Sec. 2 we summarize the main definitions and describe the numerical setup. In Sec. 3 we discuss in detail a representative model, while Sec. 4 presents the main properties of a sequence of models with constant specific angular momentum. A brief discussion is found in Sec. 5.

Throughout the paper, we assume a signature of $(-, +, +, +)$ and set $c = G = 1$.

2. Tori in stationary, axisymmetric spacetimes

The details of our formalism and numerical method can be found in Ref. 31. Here we only summarize the main equations:

We assume that the spacetime is stationary and axisymmetric, with circular velocity field, while the matter is described as a perfect fluid with total energy density ϵ , rest mass density ρ and pressure p . We further assume that the torus has a constant specific angular momentum $l := -u_\phi/u_t$, where u^α is the 4-velocity. The hydrostationary equilibrium equation can be written in the form

$$\frac{\nabla p}{\epsilon + p} = -\nabla \ln(-u_t) + \frac{\Omega \nabla l}{1 - \Omega l}, \quad (1)$$

where $\Omega := u^\phi/u^t$ is the angular velocity and has a first integral only under specific conditions. For a barotropic equation of state of the form $p = p(\rho)$ one can define the log-enthalpy

$$H(p) := \int_0^p \frac{dp'}{\epsilon(p') + p'}, \quad (2)$$

with, $dH/dp = (\epsilon + p)^{-1}$. Then, the l.h.s. of (1) becomes $(\epsilon + p)^{-1} \nabla p = \nabla H$ and if $\Omega = \Omega(l)$, we can write

$$\nabla H = -\nabla W, \quad (3)$$

where $-\nabla W$ is the effective gravity, given by the gradient of the effective potential

$$W = \ln(-u_t) - \int^l \frac{\Omega}{1 - \Omega l} dl + \text{const.} \quad (4)$$

It follows that the surfaces of constant pressure coincide with the equipotential surfaces and at the location of maximum density, $\nabla H = \nabla W = 0$ (the constant in (4) can be set by requiring that W vanishes at infinity).

For the case of constant specific angular momentum the first integral of (1) becomes

$$H + \ln(-u_t) = \text{const.} \quad (5)$$

and for the homentropic, polytropic equation of state (EOS)

$$p = K \rho^\Gamma, \quad (6)$$

$$\epsilon = \rho + \frac{p}{\Gamma - 1}, \quad (7)$$

where K is the polytropic constant and Γ is the polytropic exponent, one obtains

$$H = \ln[1 + \Gamma/(\Gamma - 1)K\rho^{\Gamma-1}], \quad (8)$$

The density distribution is given algebraically, as an implicit function of Ω (for given EOS, l_0 , inner radius r_{in} and stationary, axisymmetric spacetime):

$$\rho = \left\{ \frac{\Gamma - 1}{K\Gamma} \left[\frac{u_{t,\text{in}}}{u_t} - 1 \right] \right\}^{\frac{1}{\Gamma-1}}. \quad (9)$$

For our self-consistent numerical scheme we use the analytic AJS solutions²⁵ as an initial guess. In isotropic coordinates (t, r, θ, ϕ) , the metric of the Schwarzschild spacetime is

$$ds^2 = - \left[\frac{1 - M/2r}{1 + M/2r} \right]^2 dt^2 + \left(1 + \frac{M}{2r} \right)^4 (dr^2 + r^2 d\theta^2 + r^2 \sin^2 \theta d\phi^2), \quad (10)$$

where the isotropic radial coordinate r is related to the Schwarzschild radial coordinate \mathfrak{r} by $r = 1/2 [\mathfrak{r} - M + \sqrt{\mathfrak{r}^2 - 2M\mathfrak{r}}]$. Requiring $W(r = \infty) = 0$, the effective potential is

$$W = \ln(-u_t). \quad (11)$$

A torus of finite size extends between $r = r_{\text{in}}$ and $r = r_{\text{out}}$ in the equatorial plane. At the density maximum, $\nabla_r p = 0$ and the fluid elements there move as free test particles with Keplerian angular momentum

$$l_{\text{K}} = \frac{\sqrt{M} (1 + M/2r)^6 r^2}{(1 - M/2r)^2 (M + M^2/4r + r)^{3/2}}, \quad (12)$$

has a minimum at the marginally stable circular orbit for test particles, $r_{\text{ms}} = 1/2(5 + 2\sqrt{6}) \simeq 4.950$, which restricts $r_{\text{max}} > r_{\text{ms}} \Rightarrow l > l_{\text{ms}} = 3.674M$. The radius of the marginally bound orbit is the location where $W = 0$ for $l = 4M$, i.e. $r_{\text{mb}} \simeq 2.914$. The largest of three roots of $l = l_{\text{K}}$ corresponds to $r = r_{\text{max}}$, while the intermediate root, $r = r_{\text{cusp}}$, corresponds to the existence of a cusp, where again $\nabla_r p = 0$. For a given EOS and black-hole mass M and for a given value of l , there exists a one-parameter family of different finite-size tori with $r_{\text{cusp}} < r_{\text{in}} < r_{\text{max}}$, which all have the same r_{max} . For a chosen r_{in} in this range, one obtains the density distribution from (9). The parameter space of possible equilibrium configurations is further limited by the existence of the marginally bound orbit, r_{mb} . For $l < l_{\text{mb}} = 4M$, the effective potential W is always negative in the equatorial plane, while for $l = l_{\text{mb}}$, $W = 0$ at r_{mb} (an inflection point) and the location of the cusp is at $r_{\text{in}} = r_{\text{mb}}$. For $l > l_{\text{mb}}$ there exists a region in the equatorial plane with $W > 0$. Thus, for any $l > l_{\text{mb}}$, only tori without a cusp are possible, with the inner radius limited by the location of $W = 0$.

For self-gravitating tori, we use the metric in quasi-isotropic coordinates

$$ds^2 = -e^{2\nu} dt^2 + e^{2\alpha} (dr^2 + r^2 d\theta^2) + e^{2(\gamma-\nu)} r^2 \sin^2 \theta (d\phi - \omega dt)^2, \quad (13)$$

where ν, γ, α and ω are metric functions that depend only on the coordinates r and θ (see Ref. 32). Because γ and ν are divergent at the event horizon, we will use, instead, the functions²⁷ $B := e^\gamma$ and $\lambda := e^\nu$, with boundary conditions on the event horizon $B = 0$, $\lambda = 0$ and $\omega = \omega_h$, where ω_h is the constant angular velocity of the horizon. The horizon can be chosen to be a sphere of constant radius $r = h_0$. On the axis of rotation, the condition $\alpha = \gamma - \nu$ ensures local flatness.

In the angular direction we use the coordinate $\mu := \cos \theta$ instead of θ , while in the radial direction we use a compactified, nondimensional coordinate s , defined

through

$$r := r_e \frac{s}{1-s}, \quad (14)$$

where r_e is a suitably chosen radius (here we use $r_e = r_{\text{out}}$, so that the outer edge of the torus in the equatorial plane corresponds to $s = 0.5$). Through this compactification, the infinite domain $r \rightarrow [0, +\infty)$ is mapped onto the finite domain $s \rightarrow [0, 1]$. The location of the horizon is at $s = s_0$, so that $h_0 = r_e s_0 / (1 - s_0)$.

The field equations for the three metric functions λ , B and ω are of elliptic type

$$\nabla^2 \lambda = S_\lambda(s, \mu), \quad (15)$$

$$\left(\nabla^2 + \frac{(1-s)^3}{r_e^2 s} \frac{\partial}{\partial s} - \frac{(1-s)^2}{r_e^2 s^2} \mu \frac{\partial}{\partial \mu} \right) B = S_B(s, \mu), \quad (16)$$

$$\left(\nabla^2 + \frac{2(1-s)^3}{r_e^2 s} \frac{\partial}{\partial s} - \frac{2(1-s)^2}{r_e^2 s^2} \mu \frac{\partial}{\partial \mu} \right) \omega = S_\omega(s, \mu), \quad (17)$$

where ∇^2 is the flat-space Laplacian, and S_λ , S_B and S_ω are source terms. These elliptic-type equations are inverted using appropriate Green's functions, while the equation for the metric function α is integrated as an ordinary differential equation.

While we use nondimensional units of $c = G = M_{\text{BH}}^{\text{AJS}} = 1$ in the numerical procedure, the solution can then be scaled to any desired black hole mass. Our grid is equidistant in (s, μ) with 2001×1001 grid points. For a chosen polytropic index Γ , the solution space of AJS models is three-dimensional: the parameter l controls the rotation of the torus, r_e/h_0 controls its size and K (or ρ_{max}) its mass (through the variation of the equation of state).

Our fixed-point-iteration method is described in detail in Ref. 31. Here, we note that our numerical procedure yields directly a self-consistent model, starting from the AJS solution as an initial guess. In order to construct models that exactly fill their Roche lobe, we must be able to compute models that violate this limit, in order to approach it by bisection. For this purpose, we also construct models starting with an AJS solution that overfills the Roche lobe, i.e. with a value of W_{in} larger than W_{cusp} , but truncated at r_{cusp} (similar models were constructed in other works, in order to initiate mass accretion onto the black hole). Exploring the allowed parameter range, we then find models that exactly fill their Roche lobe, up to a single grid point.

3. A representative model

A representative solution is constructed for a polytropic equation of state with index $N = 3$ and constant $K/M_{\text{BH}}^{2/N} = 17.34$, a ratio of outer torus radius to horizon radius $r_e/h_0 = 49$ and with $\omega_h = 0$. The specific angular momentum in the initial guess is $l/M_{\text{BH}}^{\text{AJS}} = 3.675$, while it is $l/M_{\text{BH}} = 3.911$ in the converged, self-consistent solution. A detailed list of various properties, scaled by the mass of the black hole, is displayed in Table 1 (see Ref. 31 for definitions). The ratio of torus mass to black hole mass is $M_{\text{T}}/M_{\text{BH}} = 0.21$, while the total mass of the spacetime is

Table 1. Properties of a representative self-consistent model of a BH-torus system, with $N = 3$, $l/M_{\text{BH}}=3.911$, $r_{\text{out}}/h_0=49.005$, $\omega_h = 0$ and $K/M_{\text{BH}}^{2/N}=17.339$. All radii are coordinate radii in the quasi-isotropic metric.

Asymptotic spacetime mass	M/M_{BH}	1.1730
Torus mass	$M_{\text{T}}/M_{\text{BH}}$	0.2097
Maximum density	$\rho_{\text{max}}M_{\text{BH}}^2$	6.6126×10^{-5}
Inner torus radius	$r_{\text{in}}/M_{\text{BH}}$	3.0413
Radius of maximum density	$r_{\text{max}}/M_{\text{BH}}$	8.1931
Outer torus radius	$r_{\text{out}}/M_{\text{BH}}$	23.6400
Torus rest mass	M_0/M_{BH}	0.1964
Torus internal energy	$U_{\text{T}}/M_{\text{BH}}$	2.9878×10^{-3}
Torus rotational energy	$T_{\text{T}}/M_{\text{BH}}$	9.5559×10^{-3}
Torus gravitational potential energy	$W_{\text{T}}/M_{\text{BH}}$	-3.5865×10^{-2}
Torus rotational to potential energy	$ T/W _{\text{T}}$	0.2664
Torus angular momentum	$J_{\text{T}}/M_{\text{BH}}^2$	0.7390
Black hole horizon radius	h_0/M_{BH}	0.4824
Black hole Komar charge	$M_{\text{H}}/M_{\text{BH}}$	0.9633

$M/M_{\text{BH}}=1.17$. In these coordinates, the horizon of the black hole is at a radius of $h_0/M_{\text{BH}}=0.482$ (compared to 0.5 for the AJS solution). The torus itself extends from $r_{\text{in}}/M_{\text{BH}}=3.04$ to $r_{\text{out}}/M_{\text{BH}}=23.64$. The relation $M_{\text{H}}/M_{\text{BH}} < (M - M_0)/M_{\text{BH}} < 1$ holds as expected²⁹.

Notice that, the gravitational potential energy of the torus is

$$W_{\text{T}} := M - M_{\text{BH}} - M_0 - T_{\text{T}} - U_{\text{T}}, \quad (18)$$

and includes both self-energy and binding energy between the black hole and the torus. While all previous quantities are determined with high accuracy (as was checked by proper convergence studies with grids of different sizes), this is not the case for W_{T} , since it results as the difference between considerably larger quantities. Even for the largest-size grid we can afford at present, a convergence study showed that the numerical error in W_{T} can range from a few % up to roughly 10%, depending on the mass of the torus. This affects also the ratio $|T/W|_{\text{T}}$. We will thus report these two quantities only up to such an uncertainty.

The four panels in Fig. 1 show the distribution of the four metric functions α , B , λ and ω , as a function of the nondimensional compactified coordinate s in the equatorial plane (we remind here that the outer radius of the torus is at $s = 0.5$). The first three functions (solid lines) are compared to the corresponding Schwarzschild solution. The largest impact of the self-gravity of the torus is in the metric function λ , while B remains largely unaffected. The metric function ω vanishes for the Schwarzschild metric, while in the self-consistent solution it shows a peak inside the torus. At the horizon and at infinity, all metric functions attain their expected boundary values, enforced by the Green's functions approach.

Fig. 2 shows the isocontours of the effective potential W in Cartesian coordinates (X, Z) scaled by the outer radius of the torus. For this particular model the marginally bound isocontour, $W = 0$, does not cross the equatorial plane. Instead,

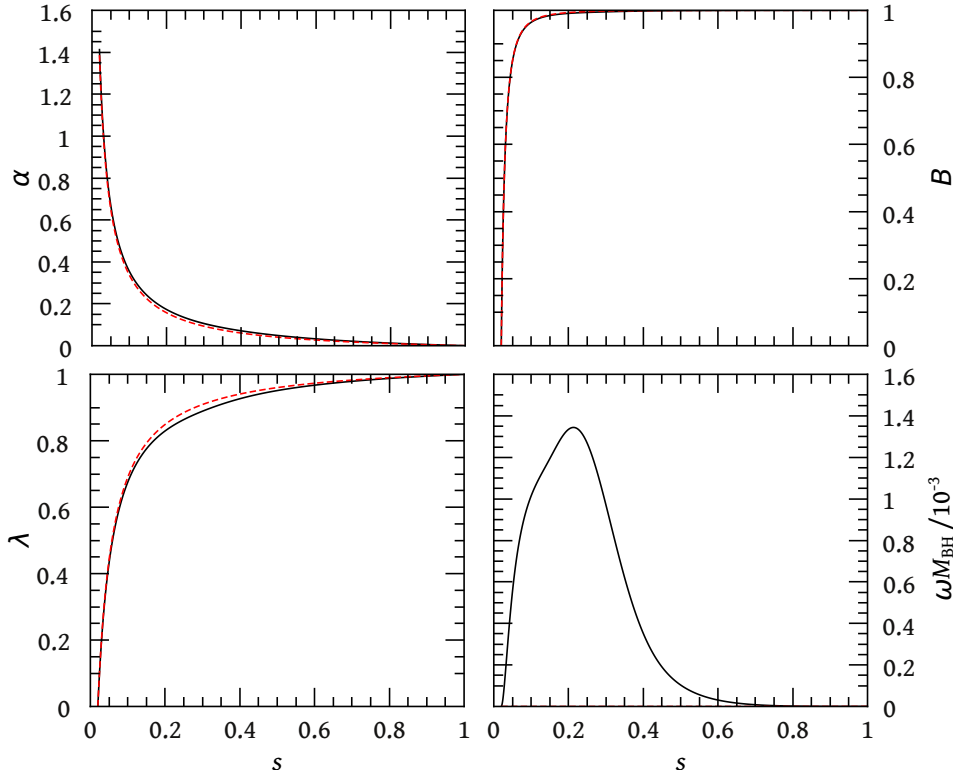


Fig. 1. Distribution of the four metric functions of the representative model of Table 1 in the equatorial plane (solid lines), as a function of the nondimensional compactified coordinate s (the outer edge of the torus is at $s = 0.5$). The horizon of the black hole is at $s_0 = 0.02$. The corresponding Schwarzschild solution (the spacetime used in the AJS limit) is shown as dashed lines.

all isocontours that cross the equatorial plane have $W < 0$ and a cusp exists. Matter fills exactly the Roche lobe (thick black line), which has a cusp in the equatorial plane. Inside the Roche lobe, the isocontours of the effective potential W coincide with corresponding isodensity contours.

Fig. 3 shows the distribution of the effective potential W in the equatorial plane, as well as the difference of the Keplerian specific angular momentum l_K from the constant value l inside the torus. For this model with cusp, the inner edge of the torus coincides with a local maximum in W and with the location where $l_K - l = 0$. The close agreement between these two quantities demonstrates the high accuracy of the numerical solution. The radius of the marginally stable orbit, r_{ms} , corresponds to the local minimum in $l_K - l$, while the radius where the density has a maximum, r_{max} , coincides with a local minimum in W . Furthermore, at the outer radius of the torus, r_{out} , the effective potential has the same value as at the cusp.

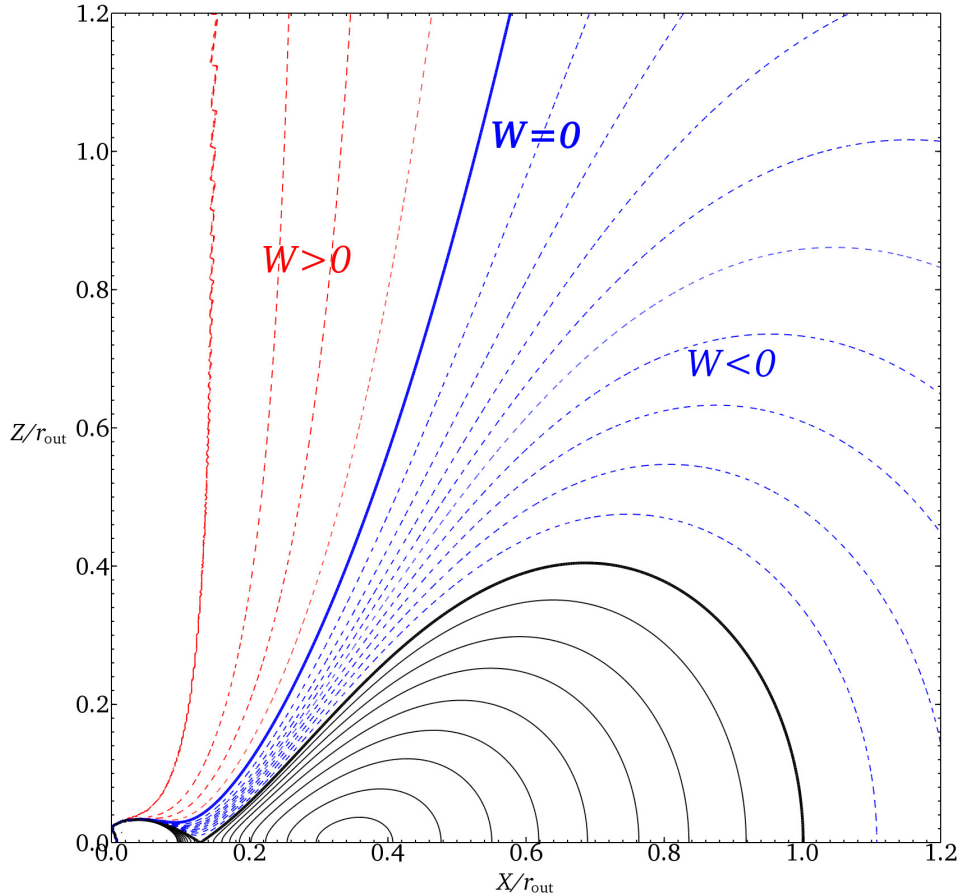


Fig. 2. Isocontours of the effective potential W , in Cartesian coordinates, scaled by the outer radius of the torus, r_{out} , for the representative model of Table 1. The torus fills exactly its Roche lobe (thick black line), which has a cusp in the equatorial plane. Inside the Roche lobe, the isocontours of W and of the density, ρ , coincide (thin black lines). Isocontours of W outside the torus can have negative or positive values (dashed lines), separated by the marginally-bound surface ($W = 0$). The horizon of the black hole is a sphere with radius $h_0/r_{\text{out}} = 0.02$ (not shown here).

4. A sequence of models with cusp

In the AJS limit, models with constant specific angular momentum are required to have $l > 3.674M_{\text{BH}}^{\text{AJS}}$, in order for a finite-size torus to exist. We construct a sequence of self-consistent models with different torus mass, that all fill exactly their Roche lobe, with $l > 3.675M_{\text{BH}}^{\text{AJS}}$. Table 2 summarizes the main properties of models belonging to this sequence, with the first line corresponding to the AJS solution (no values for M_{T} and $J_{\text{T}}/M_{\text{BH}}^2$ are given, since the AJS solution is independent of the torus mass). In the AJS limit, the torus has a very small size, extending between $r_{\text{in}}/M_{\text{BH}} = 4.84$ and $r_{\text{out}}/M_{\text{BH}} = 5.24$. In the self-consistent solution, the value

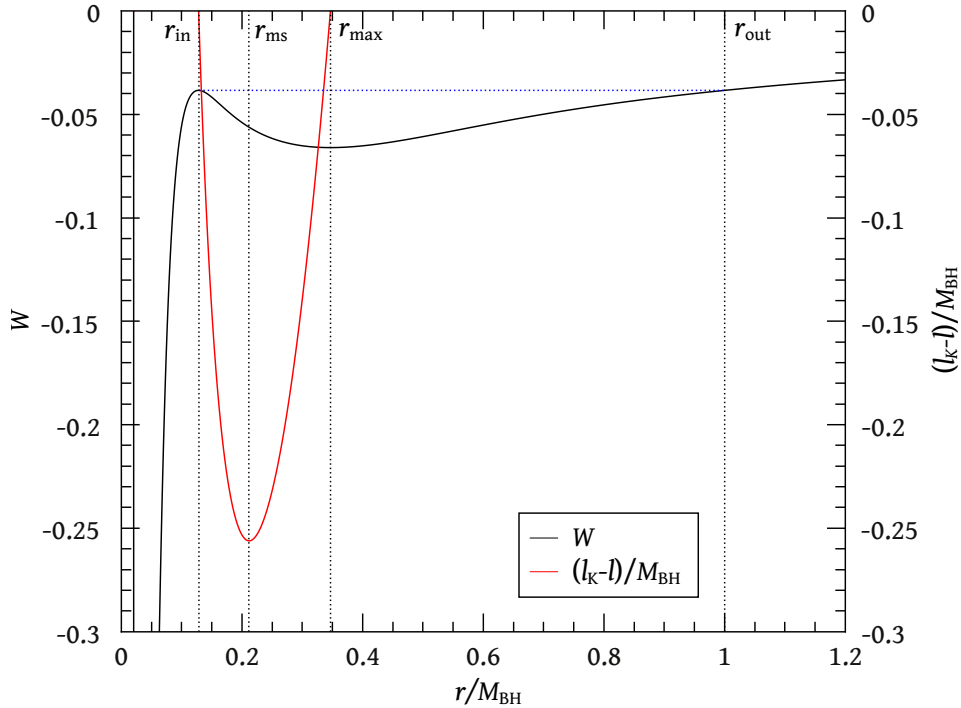


Fig. 3. The effective potential W and $l_K - l$ in the equatorial plane for the representative model of Table 1. The radius of the inner edge of the torus, r_{in} , the marginally stable orbit r_{ms} , the location of the density maximum, r_{max} , and the radius of the outer edge of the torus, r_{out} , are shown with dotted vertical lines. A dotted horizontal line connects the inner and outer edges of the torus at the same value of the effective potential.

Table 2. Properties of a sequence of models with a cusp with $N = 3$, $l/M_{\text{BH}}^{\text{AJS}} = 3.675$ and $\omega_h = 0$.

$M_{\text{T}}/M_{\text{BH}}$	M/M_{BH}	l/M_{BH}	$r_{\text{in}}/M_{\text{BH}}$	$r_{\text{max}}/M_{\text{BH}}$	$r_{\text{out}}/M_{\text{BH}}$	$J_{\text{T}}/M_{\text{BH}}^2$
–	1.000	3.675	4.838	5.092	5.244	–
0.134	1.107	3.859	3.193	7.763	18.235	0.460
0.296	1.249	3.948	2.888	8.765	39.329	1.079
0.366	1.312	3.952	2.784	9.025	58.745	1.357
0.438	1.379	3.947	2.723	9.167	85.049	1.644
0.546	1.484	3.948	2.660	9.293	133.360	2.074

of l/M_{BH} changes, but in the last four models of the sequence it stays practically constant at $l/M_{\text{BH}} = 3.95$. Increasing the mass of the torus only increases the total mass-energy of the spacetime, but not the mass of the BH. Along the sequence, the radius of the inner edge of the torus decreases, approaching the horizon, while the radius of the maximum density increases. The most dramatic increase is in the outer radius of the torus, which grows more than 25 times for the most massive model considered here, compared to the AJS limit. Part of this difference can be

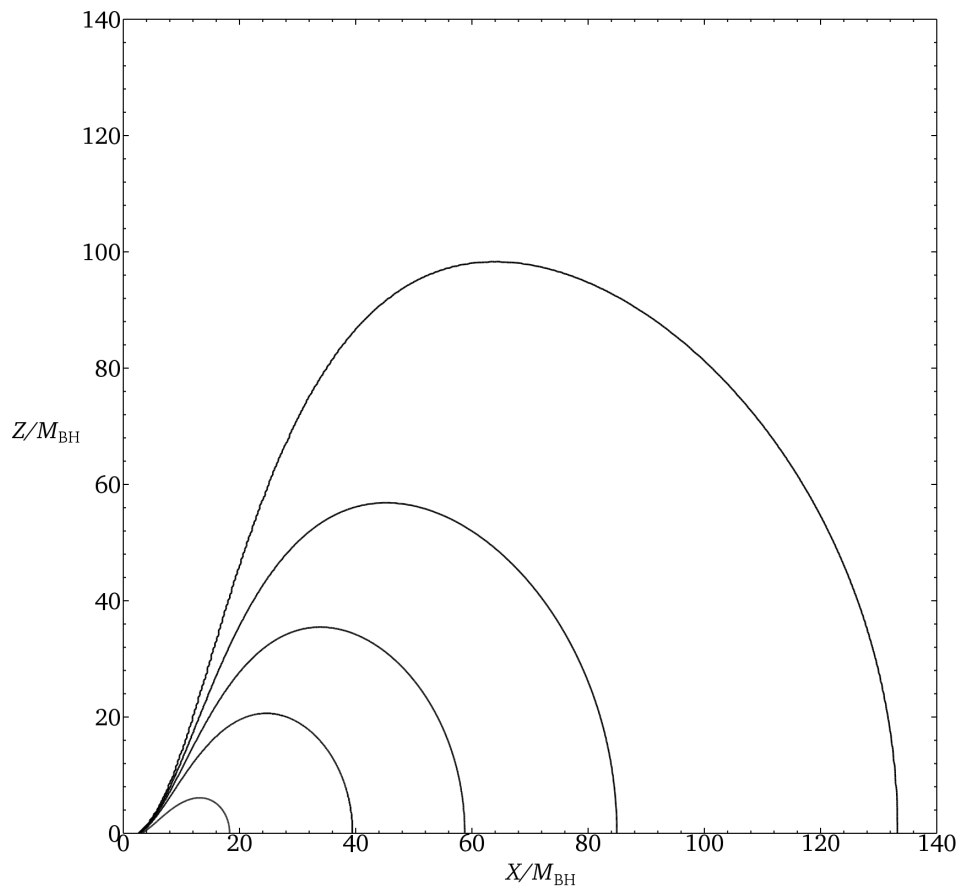


Fig. 4. Outer surface for each of the models presented in Table 2 (except for the AJS limit) in Cartesian coordinates. With increasing torus mass, the outer edge of the torus, as well as its vertical extent, increase significantly. The horizon of the black hole in each case is a sphere with radius ranging from $h_0/M_{\text{BH}} = 0.47$ (largest torus) to $h_0/M_{\text{BH}} = 0.49$ (smallest torus) and is not shown here.

attributed to the fact that l/M_{BH} increases. Nevertheless, the last four models in Table 2 constitute a proper sequence of models with practically the same l/M_{BH} , so they can be compared on an equal footing. Among these models, the outer radius also increases significantly with increasing mass of the torus. This can be seen in more detail in Fig. 4, which compares the structure of the different tori in Table 2 (showing only the surface for each model), in Cartesian coordinates scaled by M_{BH} . The total vertical extent of the torus approaches twice its extent in the equatorial plane, as the torus mass increases.

Fig. 5 shows the effective potential in the equatorial plane, for the sequence of models in Table 2. As the torus mass increases, the value of the effective potential at the inner edge of the torus, W_{in} , (shown with a dashed line connecting the

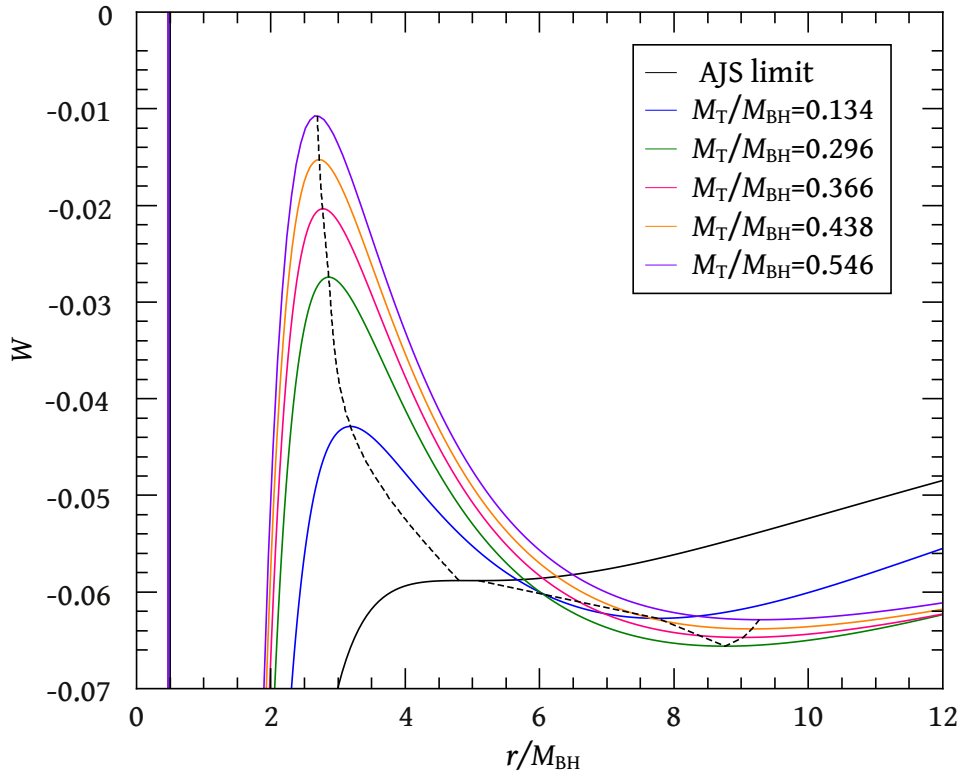


Fig. 5. The effective potential in the equatorial plane, for the sequence of models presented in Table 2. The shape of the potential changes significantly with increasing torus mass, due to self-gravity effects. A dashed line connects the local maximum for each model, that corresponds to r_{in} , while another dashed line connects the local minimum for each model, that corresponds to r_{max} .

local maxima in the effective potential) increases significantly, which can be seen in more detail in Fig. 6. It appears that W_{in} only asymptotically approaches the marginally-bound value of $W = 0$ and does not cross this limit. This is natural, since marginally bound tori close their Roche lobe at infinity. Thus, a sequence of bound models with increasing mass would first need to reach a marginally bound state with infinite radius, before connecting to a sequence of models that have no cusp. We conclude that for tori with constant specific angular momentum, the limitation of $l < 4M_{\text{BH}}$ may also hold for self-consistent models, as it does in the AJS limit, although a more detailed investigation is needed to locate the precise limit.

5. Discussion

We present an improved method for constructing general-relativistic models of self-gravitating tori around black holes. It is a self-consistent-field method, with the field equations inverted using Green's functions and its improvement over an existing approach²⁷ consists in the use of compactified coordinates. This allows for the metric

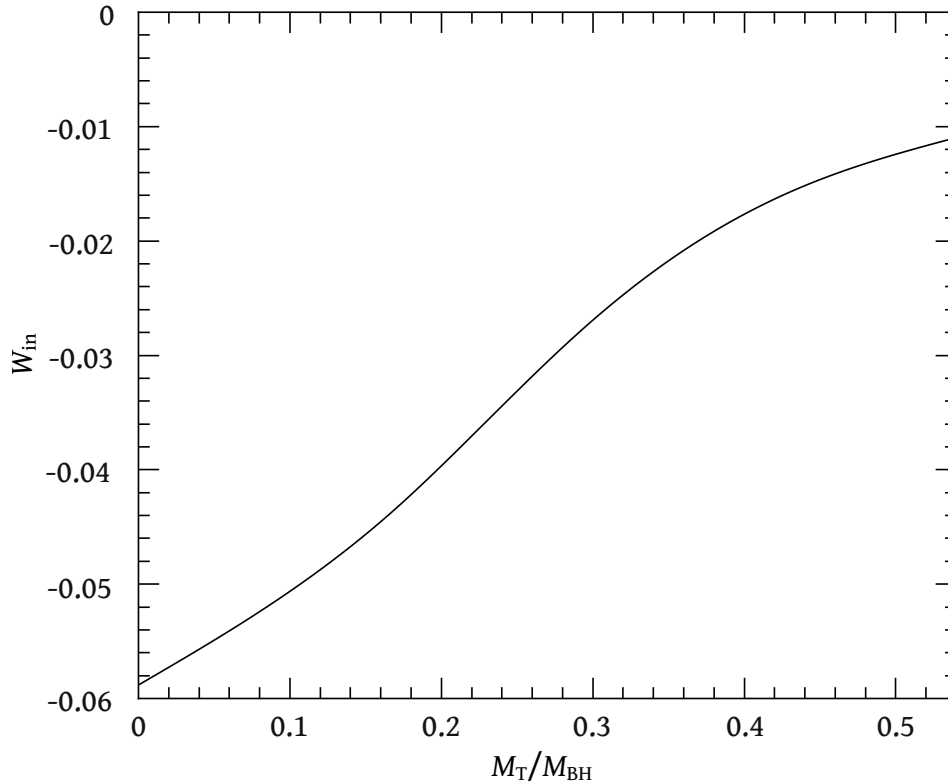


Fig. 6. The value of the effective potential W_{in} at the inner edge of the torus for the sequence of models presented in Table 2. With increasing torus mass, W_{in} approaches, but does not cross the marginally-bound value of $W_{in} = 0$.

to be computed up to spatial infinity, resulting in highly accurate initial data for numerical evolution codes. These initial data have already been used successfully in studying nonaxisymmetric instabilities in fully general-relativistic models of massive accretion tori¹². Of interest is also a more detailed study of the precise conditions under which the axisymmetric runaway instability is active, since the numerical code is highly accurate and robust, allowing for the construction of models that exactly fill their Roche lobe, when a cusp exists.

Scaling all results with the mass of the black hole, we found evidence that models with constant specific angular momentum that can fill their Roche lobe are still limited by $l < 4M_{BH}$ (as is the case for models constructed in a fixed background metric) even for heavy tori. The precise limit must be determined with a more detailed study. More generally, we plan to investigate the allowed parameter space for different types of self-gravitating tori, including the case of rotating black holes and more general rotation laws and equations of state.

Acknowledgments

I would like to thank Burkhard Zink, Oleg Korobkin and Marcus Ansorg for useful discussions and I'm grateful to the University of Tuebingen for hospitality during an extended visit.

References

1. Woosley S E 1993 *Astrophys. J.* **405** 273
2. Woosley S E and Bloom J S 2006 *Annual Rev. Astron. Astrophys.* **44** 507
3. Ruffert M, Janka H Th and Schäfer G 1996 *Astron. Astrophys.* **311** 532
4. Duez M D 2010 *Class. Quant. Grav.* **27** 114002
5. Rezzolla L, Baiotti L, Giacomazzo B, Link D and Font J A 2010 *Class. Quant. Grav.* **27** 114105
6. Shibata M and Taniguchi K 2006 *Phys. Rev. D* **73** 064027
7. Shibata M, Kyutoku K, Yamamoto T and Taniguchi K 2009 *Phys. Rev. D* **79** 044030
8. Papaloizou J C B and Pringle J E 1984 *Mon. Not. R. Astron. Soc.* **208** 721
9. Papaloizou J C B and Pringle J E 1985 *Mon. Not. R. Astron. Soc.* **213** 799
10. Kojima Y 1986 *Prog. Theor. Phys.* **75** 251
11. Woodward J W, Tohline J E and Hachisu I 1994 **420** 247
12. Korobkin O, Abdikamalov E B, Schnetter E, Stergioulas N and Zink B 2010 *Phys. Rev. D* **83** 043007
13. Abramowicz M A, Calvani M and Nobili L 1983 *Nature* **302** 597
14. Font J A and Daigne F 2002 *Mon. Not. R. Astron. Soc.* **334** 383
15. Daigne F and Font J A *Mon. Not. R. Astron. Soc.* **349** 841
16. Daigne F and Mochkovitch R *Mon. Not. R. Astron. Soc.* **285** L15
17. Abramowicz M A, Karas V and Lanza A 1998 *Astron. Astrophys.* **331** 1143
18. Lu Y, Cheng K S, Yang L T and Zhang L *Mon. Not. R. Astron. Soc.* **314** 453
19. Zanotti O, Font J A, Rezzolla L and Montero P 2005 *Mon. Not. R. Astron. Soc.* **356** 1371
20. Nishida S and Eriguchi Y 1996 *Astrophys. J.* **461** 320
21. Nishida S, Lanza A, Eriguchi Y and Abramowicz M A 1996 *Mon. Not. R. Astron. Soc.* **278** L41
22. Masuda N and Eriguchi Y 1997 *Astrophys. J.* **489** 804
23. Masuda N, Nishida S and Eriguchi Y 1998 *Mon. Not. R. Astron. Soc.* **297** 1139
24. Montero P J, Font J A, Shibata M 2010 *Phys. Rev. Letters* **104** 191101
25. Abramowicz M, Jaroszynski M and Sikora M 1978 *Astron. Astrophys.* **63** 221
26. Kozłowski M, Jaroszyński M and Abramowicz M A 1978 *Astron. Astrophys.* **63** 209
27. Nishida S and Eriguchi Y 1994 *Astrophys. J.* **427** 429
28. Ansorg M and Petroff D 2005 *Phys. Rev. D* **72** 024019
29. Shibata M 2007 *Phys. Rev. D* **76** 064035
30. Cook G B, Shapiro S L and Teukolsky S A 1994 *Astrophys. J.* **422** 227
31. Stergioulas N 2011 *J. Phys. Conf. Ser.* **283** 012036
32. Stergioulas N 2003 *Living Rev. Relativity* **6** 3